Activation of the Crtc2/Creb1 transcriptional network in skeletal muscle enhances weight loss during intermittent fasting

Nelson E. Bruno[1]*, Jerome C. Nwachukwu[1], Sathish Srinivasan[1], Richard Hawkins, David Sturgill[3], Gordon L. Hager[3], Stephen Hurst[4], Shey-Shing Sheu[4], Michael D. Conkright[5], Kendall W. Nettles[1]*

[1]Department of Integrative Structural and Computational Biology, The Scripps Research Institute, 130 Scripps Way, Jupiter FL 33458, USA

[2]Department of Cancer Biology, The Scripps Research Institute, 130 Scripps Way, Jupiter FL 33458, USA

[3]Laboratory of Receptor Biology and Gene Expression, National Cancer Institute, NIH, Bethesda, MD 20892, USA

[4]Center for Translational Medicine, Department of Medicine, Thomas Jefferson University, Philadelphia, PA, 19107, USA.

[5]Department of Shared Services, The Scripps Research Institute, 130 Scripps Way, Jupiter FL 33458, USA

Correspondence: Nelson E Bruno, nbruno@scripps.edu; Kendall Nettles, knettles@scripps.edu

Conflict of interest statement: The authors declare no conflicts of interest.

Abstract

Exercise is a behavior modification indispensable for long-term weight loss. Exercise activates the Creb-Regulated Transcriptional Coactivator (Crtc) family of transcriptional coregulators to drive Creb1-mediated anabolic transcriptional programs in skeletal muscle. Here, we show that induced overexpression of a skeletal muscle specific Crtc2 transgene in aged mice leads to greater weight loss during alternate day fasting, and selective loss of fat rather than lean mass. Transcriptional profiling revealed that fasting and weight loss downregulated most of the mitochondrial electron transport genes and other regulators of mitochondrial function that were substantially reversed in the Crtc2 mice, which maintained higher energy expenditure during fasting. The Crtc2 mice displayed greater mitochondrial activity, metabolic flux capacity for both carbohydrates and fats, improved glucose tolerance and insulin sensitivity, and increased oxidative capacity before the fast, suggesting muscle-intrinsic mechanisms in support of improved weight loss. This work reveals that Crtc2/Creb1-mediated signaling coordinates metabolic adaptations in skeletal muscle that explain how Crtc2/Creb contribute to the effects of exercise on metabolism and weight loss.

Introduction

Long-term dieting is usually not effective in maintaining a lower body weight due to increased hunger and a slower metabolic rate (1). In humans, loss of >10% of body weight also increases metabolic efficiency, such that ~500 less calories per day are required to maintain the same energy expenditure (2). Weight loss reduces the metabolic rate due to a number of changes including increased circulating leptin and decreased thyroid hormone and sympathetic nervous system (SNS) activity (2-4). People who maintain long-term weight loss almost invariably exercise (5), and both preclinical and clinical data suggest that this is through raising metabolic rate (6-8), decreased energy efficiency (9), and increased energy expenditure from the increased physical activity (10).

Creb1-regulated transcription is stimulated by GPCRs that activate adenylyl cyclases to convert ATP to the second messenger cAMP, which in turn liberates the catalytic subunit of protein kinase A (PKA) (11). Crtc1–3 family members are primary coactivators for Creb1 that are also highly conserved in the cAMP transcriptional response. Crtc1–3 are rendered cytoplasmic and inactive by phosphorylation (12). In contrast, they are fully activated through synergistic dephosphorylation by phosphatases downstream of PKA and calcium flux in polarizable tissues including the skeletal muscle (13), hippocampus (14), cortex (15), islet cells (12), and the renal proximal tubule (16). In skeletal muscle, Crtc/Creb1 is activated by exercise downstream of the β-adrenergic receptor and calcium flux, stimulating anabolic transcriptional programs, including induction of PGC-1α (13, 17) and in vitro enhancement of oxidative capacity (17). These training adaptations lead to significant enhancement of high intensity exercise performance along with greater glycogen and intramuscular triglyceride stores (13). While Crtc/Creb1 coordinates metabolic transcriptional programs in other tissues such as adipocytes, liver, and pancreas, its role in skeletal muscle metabolism has not been studied in vivo.

60 To investigate the effects of Crtc2/Creb1 activation in adult skeletal muscle, we generated
61 doxycycline (dox)-inducible transgenic mice that show skeletal muscle-specific overexpression of
62 Crtc2 (FLAG-Crtc2 S171A/S275A/K628R mutant that prevents cytoplasmic localization) under
63 the control of a tetracycline response element (13). Given the primary role of exercise adaptations
64 in regulating whole-body metabolism, we examined here the role of the Crtc2/Creb1
65 transcriptional network in skeletal muscle metabolism during alternate day fasting (ADF),
66 mimicking a common dieting scheme in humans. Activation of Creb1-regulated transcriptional
67 responses during fasting enabled maintenance of a lower body weight due to the stimulation of
68 higher energy expenditure and other metabolic changes, enabling selective loss of fat mass and
69 retention of lean mass, as observed in humans who exercise (18, 19). Crtc2 mice displayed the
70 metabolic hallmarks of an exercised phenotype, including enhanced mitochondrial activity,
71 improved lipid and carbohydrate flux capacity and storage, and insulin sensitization. These data
72 support a model where lower metabolic activity during fasting and weight loss contributes to
73 weight regain, which can be reversed by exercise-induced activation of Crtc2/Creb1-regulated
74 transcriptional programs.
75
76 **Results**
77 **Crtc2 overexpression in skeletal muscle facilitates weight loss**
78 We studied aged Crtc2 (rtTA/Crtc2^{tm}) or WT (rtTA/WT) mice, which in the C57BL/6 background
79 naturally gain fat mass as they age (18 weeks, 30–39 g, **Figure 1A–B**). During dox treatment,
80 Crtc2 mice gained weight similarly to control WT mice (**Figure S1A**). On the ADF protocol, three
81 separate cohorts of Crtc2 mice displayed significantly greater and sustained weight loss than WT
82 mice, with Crtc2 mice losing about twice as much weight in each case, 9-14% of body weight

83 (**Figure 1C, Figure S1B**).

84 After 3 weeks of ad libitum refeeding, the Crtc2 mice re-gained more weight to catch up
85 with the WT mice (**Figure 1D**), which may be due to the anabolic effects of higher insulin
86 sensitivity, described below. We found that locomotion was similarly reduced in both groups
87 during the refeeding period (**Figure S1C**), the number of meals doubled in both groups, while
88 meal duration and number of bouts per meal declined similarly (**Figure 1E**). We observed a
89 reduction in kilocalories consumed in the Crtc2 relative to the WT group, which planned
90 comparisons demonstrated was significant only during the second ADF cycle, when the WT mice
91 increased consumption at a faster rate than the Crtc2 mice (**Figure 1E**). Increases in skeletal muscle
92 storage of glycogen and triglycerides associated with the anabolic phenotype of Crtc2/Creb1
93 activation (13) likely contributed to the early response to fasting, perhaps explaining the initially
94 slower rate of increased food consumption in the Crtc2 mice. These differences in caloric
95 consumption are consistent with the differences in body weight between cohorts and disappear
96 after normalization for body weight. Control mice lost more lean mass, while Crtc2 mice
97 conserved lean mass and burned the excess fat accumulated during aging (**Figure 1F**), similar to
98 the effects of exercise (20). To verify that Crtc2 helps maintain lower body weight in a different
99 model, we placed mice on a high fat diet, and found that Crtc2 mice also maintained lower body
100 weight than WT mice in this context (**Figure 1G**). Thus, the activation of Crtc2/Creb1 signaling
101 in skeletal muscle significantly modulated body composition and weight loss, mimicking the
102 effects of exercise training including preferential loss of fat mass.

103

104 **The transcriptional response to fasting and weight loss and its regulation by Crtc2**

105 To understand the skeletal muscle intrinsic effects of Crtc2 on dieting and weight loss, we performed

106 transcriptional profiling of mice tibialis anterior (TA) muscles electroporated with control and Crtc2
107 expression plasmids in contralateral legs. One cohort of electroporated mice was subject to 3 cycles
108 of ADF, while the other cohort was fed ad libitum. TA muscle tissues were collected from both
109 cohorts at the end of the third 24-hr fast. The transduction increased *Crtc2* mRNA levels by ~2.5-
110 fold across groups (**Figure S2A**). In response to ADF, we identified 1,880 differentially expressed
111 genes (DEGs) in the control-transduced muscle and 3,197 DEGs in Crtc2-transduced muscle, with
112 1,380 genes in common between the two groups (**Figure S2B, Supplementary Dataset_1**).
113 Analysis of canonical signaling pathways and gene ontology (GO) annotations revealed that ADF
114 modulated the transcriptional programs for lipid and carbohydrate metabolism, fatty acid beta-
115 oxidation, and insulin signaling (**Figure S2C-D**). ADF also regulated transcriptional programs that
116 control protein balance, including autophagy and ubiquitin-dependent proteasomal degradation,
117 RNA splicing, and transcription (**Figure S2C-D, Supplementary Dataset_1**). There were also over
118 200 DEGs regulated by ADF that were annotated as transcription factors and transcriptional
119 coregulators along with > 50 transcription factor and coregulators altered by Crtc2 over-expression
120 (**Figure S2E-G, Supplementary Dataset_1)**.
121

122 **Crtc2 reverses fasting- and weight loss-induced effects on mitochondria and energy**
123 **expenditure**

124 In addition to lower metabolic rate, fasting and weight loss render humans and other mammals more
125 energetically efficient, such that the same amount of work is performed with less ATP production,
126 suggesting a remodeling of glycolytic or oxidative capacity (2, 21). ADF modulated the expression
127 of >200 genes whose proteins localize in mitochondria according to MitoCarta (22) (**Figure 2A**).
128 ADF downregulated most of the genes that encode the electron transport chain (complexes I–IV),

129 the ATP synthase (complex V), the mitoribosome, and the cytosolic ribosome (**Figure 2A-C**, **Figure**
130 **S3A**), but significantly upregulated genes such as *Sdha*, *Uqcrc1*, and *Atp5a1* (**Figure 2B**, **Figure**
131 **S3A**).

132 We observed a significant ADF-induced expression of genes encoding ROS scavenger
133 proteins such as thioredoxin (*Txnrd1*) and catalase (*Cat*), and genes regulating mitochondrial
134 stability*, Tomm7, Timm9,* and the AAA protease *Spg,7* known to be active during the removal of
135 damaged mitochondrial proteins (**Figure 2D**). Among the ATP synthase genes, there was a more
136 pronounced loss of gene expression in the lateral stalk genes (**Figure 2B**), which may decrease the
137 conductance of mitochondrial permeability transition pore (mPTP) and thus protect mitochondria
138 from detrimental swelling and oxidative injury (23). ADF also induced increases in mitochondrial
139 fusion (*Mfn2* and *Opa1)*, and decreased fission (*Fis)* gene expression, consistent with the protective
140 effects of fusion during nutrient deprivation (24). These adaptations could be advantageous for
141 weight loss as they prepare the mitochondria for the reduced metabolic rate and increased reliance
142 on lipid metabolism during fasting, without causing permanent damage to the mitochondrial pool
143 within the cell.

144 In mice subjected to ADF, Crtc2 transduction altered expression of 80 genes whose proteins
145 localize in the mitochondria. Crtc2 expression strongly attenuated the ADF-dependent repression of
146 electron transport chain genes and the mitoribosome (**Figure 2A–C**, **Figure S3A**), and generally
147 upregulated the other genes encoding proteins that localize to mitochondria. In addition, Crtc2
148 enhanced expression of ribosomal genes that facilitate mitoribosome assembly, and genes such as
149 *Spg7, Pink1, RhoT2*, and *Chchd3* that control the quality of mitochondrial proteins, but blocked
150 ADF-dependent downregulation of *Minos1*, a central component of the mitochondrial inner
151 membrane organizing system (**Figure 2D**). Crtc2 also upregulated expression of *Tefm*, the

152 mitochondrial transcriptional elongation factor, and *Bola3*, which participates in electron transport
153 chain assembly (25).

154 To understand how ADF affects mitochondria, we noted that glucocorticoids (GCs) are
155 one of the primary drivers of catabolic changes during fasting, and in response to ADF and Crtc2
156 overexpression, we observed over a thousand DEGs that were annotated as "glucocorticoid
157 response" genes (**Figure S2C**). In the context of an overnight fast, treatment with Dex more than
158 doubled loss of lean mass (**Figure 2E**). Using high-content imaging, we observed that Dex reduced
159 the diameter and mitochondrial potential of nutrient-deprived primary mouse skeletal myotubes
160 (**Figure 2F**). GCs can also activate the master energy sensor, AMP-activated protein kinase
161 (AMPK) (26), which can act as a glucocorticoid receptor (GR) coactivator (27). AMPK is
162 activated by a lower ATP/ADP ratio during fasting to inhibit anabolism and stimulate catabolic
163 processes such as autophagy and mitophagy. In primary myotubes, we observed a Dex-dependent
164 activating phosphorylation of AMPK that increased over time, consistent with an underlying
165 transcriptional mechanism (**Figure 2G**). Activation of AMPK with both Dex and the AMP analog,
166 AICAR, had an additive detrimental effect on myotube diameter (**Figure 2H**), suggesting that GR
167 collaborates with AMPK to drive skeletal muscle atrophy.

168 We also observed that ADF modulated the expression of genes encoding three of the
169 AMPK subunits. Changes in subunit composition are known to alter the regulation, substrate
170 preferences, and cellular location of AMPK. The α2 and β2 AMPK isoforms were significantly
171 upregulated by ADF (**Figure 2I**, SI Appendix). The α2 subunit is activated by low glycogen and
172 mediating nuclear translocation (28), while the β2 subunit is required for maintenance of muscle
173 ATP levels during fasting (29). In contrast, ADF significantly downregulated the γ3 AMPK
174 isoform (**Figure 2I**), which is required for glycogen synthesis (30), a process inhibited during

175 fasting. Thus, a combination of GR and AMPK signaling drives skeletal muscle atrophy during
176 nutrient deprivation and a loss of mitochondrial potential.

177 We further examined whether ADF- and Crtc2-induced changes in mitochondria—the
178 powerhouse of cellular respiration—are associated with changes in global energy expenditure. As
179 expected, ad libitum oxygen consumption cycled with activity in the mice, which increased at
180 night and decreased during the day (**Figure 2J, Figure S3B**). Fasting reduced oxygen consumption
181 at every cycle, and this effect was more pronounced during the day as the fast was extended
182 (**Figure S3B**). However, Crtc2 mice consistently showed higher oxygen consumption,
183 independent of fasting (**Figure 2J**).

184 When fed ad libitum, Crtc2 and control mice display similar rates of energy expenditure
185 (EE) (**Figure 2K**). We calculated EE from indirect calorimetry measurements of VO_2 and VCO_2
186 and performed ANCOVA analysis using body weight and NMR data as covariates to adjust the
187 EE to total body weight and body composition (**Figure S3C**). While fasting, the EE of WT mice
188 dropped significantly. In contrast, during fasting EE in Crtc2 mice did not drop below the ad
189 libitum levels (**Figure 2K**). Respiratory quotient was also reduced during fasting, indicating
190 greater utilization of fat for fuel, but the differences between WT and Crtc2 mice were not
191 significant (**Figure S3D–E**). These data suggest potential mechanisms to explain how physical
192 activity—through Crtc2/Creb1-regulated transcriptional programs—can help maintain a higher
193 metabolic rate and a lower body weight by upregulating expression of mitochondrial respiratory
194 chain subunits and modulating expression of other mitochondria-localized gene products, consistent
195 with the well-known beneficial effects of exercise on mitochondrial biogenesis and energy
196 expenditure.

197

198 **Crtc2 stimulates mitochondrial activity and improves oxidative capacity**

199 Prolonged fasting promotes lipolysis, insulin resistance, and mobilization of fatty acids to skeletal
200 muscle through the combined effects of glucagon and glucocorticoids on adipocytes. These actions
201 augment the rate of fatty acid oxidation by mitochondria and the ectopic accumulation of IMTGs.
202 As expected, ADF upregulated a panoply of genes involved in the transport, oxidation, and
203 esterification of fatty acids (**Figure S4A)**.

204 Crtc2 mice displayed higher oxygen consumption before the fast; therefore, we examined
205 them for improved mitochondrial function. After one week of dox treatment, Crtc2 mice showed
206 increased mitochondrial succinate dehydrogenase activity in the gastrocnemius muscle (**Figure 3A,**
207 **Figure S4B–C**) and increased expression of *Cytochrome C (Cycs)* (**Figure 3B**). Overexpression
208 of PGC-1α increases mitochondrial density and exercise performance, but without the increase in
209 metabolic rate that can occur from exercise training (31-34), highlighting the requirement for
210 additional exercised-induced signals. In addition to the previously reported direct upregulation of
211 *Ppargc1a/*PGC-1α by Crtc2 (13, 17), Crtc2 mice showed increased expression of *Nr4a3/*NOR-1
212 nuclear receptor (**Figure 3C**) which induces mitochondrial biogenesis and increases oxidative
213 capacity (35, 36), and is induced by high intensity exercise (13). Crtc2 also upregulated the *Dgat1*
214 gene (**Figure 3C**), which is a direct Creb1 target gene (13), the product of which catalyzes a rate-
215 limiting step that increases IMTG stores. These mitochondria-related genes were also upregulated
216 in primary myotubes overexpressing Crtc2, indicating a skeletal muscle-intrinsic effect of Crtc2
217 that mimics the effects of exercise (**Figure 3C**). To show that Creb1 is directly regulating atrophy,
218 we transduced primary myocytes with the dominant negative A-Creb, which reduced myotube
219 diameter (**Figure 3D**). We also observed a doubling of mitochondrial DNA after in vivo
220 electroporation of Crtc2 (**Figure 3E**). The increased mitochondrial mass was associated with

221 increased oxidative capacity, as myotubes overexpressing Crtc2 or Crtc3 oxidized more palmitate
222 than control myotubes (**Figure 3F**), as previously reported (17).
223
224 **Crtc2 improved glucose tolerance and carbohydrate metabolism before and during weight loss**
225 ADF altered regulation of a number of carbohydrate metabolism and insulin signaling genes (**Figure**
226 **S2D, Figure S5A, Supplementary Dataset_1)**. To probe for Crtc2-dependent changes in
227 carbohydrate metabolism, we performed glucose tolerance tests comparing Crtc2 and WT mice
228 following ADF or normal diet. The Crtc2 mice displayed significantly improved glucose disposal
229 after ADF, including a dramatic improvement in their ability to reduce glycemia (**Figure 4A**), and
230 required a lower insulin excursion (**Figure 4B**). Crtc2 overexpression also improved insulin
231 tolerance after fasting and weight loss (**Figure 4C**). These effects were also apparent after 1 week
232 of dox treatment in Crtc2 mice fed ad libitum (**Figure S5B–D**). In primary myotubes, expression of
233 Crtc2 was sufficient to significantly increase the uptake of 2-Deoxy-D-glucose (**Figure 4D**).
234 Crtc2 mice and Crtc2/3-overexpressing myotubes upregulated a number of carbohydrate
235 signaling genes in normal fed conditions at both the RNA and protein levels (**Figure 4E–H**),
236 including the glucose transporter, *Glut4*, whose insulin-dependent translocation to the membrane
237 drives glucose uptake into skeletal muscle, accounting for 80% of glucose disposal. The *Nr4a1* gene
238 encodes Nur77, a nuclear receptor family transcription factor that regulates transcriptional programs
239 for carbohydrate metabolism, lipolysis, and mitochondrial biogenesis (37), and is upregulated by
240 high intensity exercise or adrenergic signaling (13). *Irs2*, *Akt1*, and *Akt2* encode core components of
241 the insulin receptor signaling pathway that can coordinate anabolic signaling and improve
242 carbohydrate metabolism. We also identified a significant inhibition of myogenin expression in the
243 normal fed Crtc2 mice (**Figure 5E**), a primary driver of muscle atrophy during fasting. To validate

244 on target mechanism of action, we generated stable cell lines overexpressing Crtc3, dominant
245 negative A-Creb, or dominant negative Crtc2 expressing only the Creb binding domain (12). These
246 results demonstrate that A-Creb and dn-Crtc2 blocked basal expression of PGC-1α, Irs2, and Akt2,
247 and prevented phosphorylation of Akt1/2 at Thr308 (**Figure 4G–H**).

248 To test for pre-fasting changes in the central control of feeding and energy expenditure, we
249 completed a leptin infusion study, as leptin secretion from adipocytes both suppresses hunger and
250 stimulates the SNS. The WT and Crtc2 mice displayed identical patterns of weight loss following
251 leptin infusion (**Figure 4I**), and there were also no differences in plasma levels of feeding hormones,
252 cholesterol, or triglycerides (**Figure S5E–F**). Lastly, we considered that Crtc2 might be regulating
253 secreted proteins that modulate the response to dieting, using the Metazoan Secretome
254 Knowledgebase (38). Among 2,500 genes encoding likely secreted proteins, 171 DEGs were
255 regulated by Crtc2 during ADF. Using the Reactome.org peer-reviewed pathway database, we
256 detected significant enrichment of pathways regulating extracellular matrix, inter-cell signaling, and
257 immune function, among others (**Figure S5G**), but no changes in myokines that would drive weight
258 loss. However, Crtc2 signaling in skeletal muscle would be expected to have effects on other tissues
259 just from changes in metabolic flux, as Crtc2 mice displayed pre-fast increases in skeletal muscle
260 oxidative flux capacity.

261 This work reveals mechanisms through which diet and exercise regulate substrate mobilization
262 and metabolism and highlights how these lifestyle modifications can alter mitochondrial function,
263 energy expenditure, and the different dramatic metabolic rewiring associated with fasting versus
264 Crtc/Creb1 signals that are downstream of exercise. Reduced energy expenditure and increased
265 hunger during fasting are partly mediated by a lowering of the satiety hormone leptin, which acts
266 centrally to stimulate the SNS (2-4). Leptin is also secreted basally from adipose tissue in proportion

267 to fat mass, so it is chronically lower during fasting, which lowers sympathetic tone and energy
268 expenditure, along with reductions in circulating thyroid hormone and stimulating the HPA axis
269 (**Figure 5A**). Within skeletal muscle, increased glucocorticoids and AMPK activity are sufficient to
270 reduce mitochondrial potential (**Figure 2)**, which along with likely contributions from fasting-
271 induced lowering of thyroid hormone, βAR, and insulin receptor activity, induce mitochondrial
272 dynamics, mitophagy, and the metabolic rewiring to conserve glucose for the brain (**Figure 5A**).

273 These energetic effects are reversed by exercise (**Figure 5B**), which we now show can be
274 recapitulated by enforced expression of Crtc2/Creb1 and upregulation of mitochondrial biogenesis
275 master regulatory genes, *Essrra/*ERRα (**Figure S2E**), *Nr4a3* (NOR1) (**Figure 3B–C**),
276 *Ppargc1a/*PGC-1α (**Figure 3B**), and *Nr4a1* (NUR77) (**Figure 4E–F**). The combination of βAR and
277 Ca^{2+} signaling are required to maximally stimulate nuclear translocation of Crtc2 in skeletal muscle
278 (13). In this model, increased GC and AMPK activity during exercise promotes mitochondrial
279 dynamics, which is then coupled with mitochondrial biogenesis to increase mitochondrial potential
280 and mass, in coordination with other metabolic changes (**Figures 3–4**). Overexpression of Crtc2
281 circumvented the neuronal activation of Creb1, as Crtc2 mice had most of the hallmarks of exercise
282 adaptations before fasting and weight loss (**Figures 3–5**) (13).

283

284 **Materials and Methods**

285 **Statistical analyses**

286 Changes in body weight and body were analyzed with 2-way analysis of variance. For VO_2,
287 respiratory quotient, and ambulation data, the ad libitum and fasted periods were analyzed
288 separately with 2-way ANOVA, and the refeeding data analyzed with Student's T-test. For the
289 energy consumption data, the fasted and re-fed data were analyzed together with 2-way ANOVA.

290 Gene expression data were analyzed with 1-way ANOVA, with Dunnett's test for multiple
291 comparisons of each gene to its corresponding control. Glycemia and insulin changes over time
292 were analyzed with 2-way ANOVA, and the AUC assessed with Student's T-test. The behavioral
293 data for meal consumption were analyzed with Student's T-tests.
294

295 **Crtc2 transgenic mice and animal care**

296 All animal procedures were approved by the Scripps Research Institute ICACUC. TRE-Crtc2^{tm}
297 mice were generated by cloning FLAG-Crtc2 (S171A, S275A, K628R) into pTRE-Tight. Oocyte
298 injections were conducted into C57Bl6 at the University of Cincinnati. Double transgenic mice
299 (DTg) were generated by crossing C57BL/6-Tg(TRE-Crtc2tm)1Mdc/j mice with 1256[3Emut]
300 MCK-rtTA transgenic mice, which expresses the reverse tetracycline transactivator (rtTA)
301 regulated by the 1256[3Emut] MCK promoter specifically in skeletal muscle (Grill *et al*, 2003).
302 Wild type and TRE littermates were used as controls and treated with DOX in the same manner as
303 DTg mice. High fat diet (Research Diet D12450J) contained 60 kcal% fat and matched control low
304 fat diet (D12492) contained 10kCal% fat and 7% sucrose.
305

306 **Glucose and insulin tolerance tests**

307 Glucose tolerance testing was performed after an overnight fast. Blood glucose was quantified at
308 15, 30, 60, 90 and 120 min post-i.p. administration of 20% D-glucose (1 g/kg fasted body weight)
309 with an Accu-check glucose monitor as described (Heikkinen *et al*, 2007). Insulin tolerance testing
310 was performed on 6 hr-fasted mice injected i.p. with human insulin (1.5 U/kg fasted body weight).
311 Blood glucose levels were determined immediately before, and 15 and 30 min after, injection.
312

313 **In vivo electroporation**

314 Plasmid DNA (50 mg) was transfected into mouse tibialis anterior (TA) muscles by electroporation
315 as described previously (13). 1 hr before electroporation mice were anesthetized, and a small
316 incision was made through the skin covering the TA muscle and then injected with 30 Al of 0.5
317 U/Al hyaluronidase and then injected with plasmid DNA. *Crtc2* and *GFP* expression plasmids
318 were purified from DH5a *Escherichia coli* cultures using an EndoFree plasmid kit (Qiagen,
319 Valencia, CA, USA), and resuspended in 71 mM sterile PBS. After the injections, electric pulses
320 were administered by using non-invasive platinum-coated tweezertrodes. Eight 100-ms square-
321 wave electric pulses at a frequency of 1 Hz and at 200-ms intervals were delivered with an ECM
322 830 electroporation unit (BTX-Harvard Apparatus, Holliston, MA, USA) with a field strength of
323 40 V/cm. After the electroporation procedure, the incision was closed with Vetbond surgical glue.

324

325 **Indirect calorimetry and energy expenditure**

326 Mice were individually housed in a sixteen chamber Oxymax comprehensive lab animal
327 monitoring system (CLAMS; Columbus Instruments, Columbus OH) at 26° C. Animals were
328 allowed to acclimate for 1 day followed by VO_2 and VCO_2 were measured at 13 min intervals over
329 a continuous duration of 60 hr. Energy expenditure (EE) was calculated using the Lusk equation,
330 kcal/h = (3.815 + 1.232 × RQ) × VO_2 in l/h, where RQ is the ratio of VCO_2 to VO_2. Opto-
331 Varimetrix-3 sensor system in the *x*-, *y*-, and *z*-axes of each chamber recorded sterotype,
332 ambulatory and *z*-axis activity. Consecutive adjacent infrared beam breaks in either the *x*- or *y*-
333 axes were scored as ambulatory activity.

334

335 **Body composition**

336 Body composition was determined using time domain nuclear magnetic resonance (TD-NMR) in
337 a Bruker minispec.

338

339 **Automated food intake monitoring**

340 Feeding behavior was assessed using a BioDAQ episodic Food Intake Monitor (BioDAQ,
341 Research Diets, Inc) as described (Stengel *et al*, 2010). Feeding parameters were calculated with
342 BioDAQ Monitoring Software 2.2.02. Feeding bouts were defined as a change in stable weight
343 of food. Meals consisted of two or more bouts within 5 s with a minimum meal amount of 0.02 g.
344 Clusters of bouts occurring greater than 600 seconds apart were considered separate meals. Water
345 or water containing Dox was provided *ad libitum* from regular water bottles. Mice habituated to
346 the new environment within 1 day and showed normal food intake and regular body weight gain.

347

348 **mRNA-seq and bioinformatics**

349 Total RNA was extracted from tissues using TRIzol™ reagent (Invitrogen), and cleaned up using
350 the RNeasy kit with on-column DNA digestion (QIAGEN). Three mRNA-seq libraries per
351 condition were prepared using the NEBNext Ultra II directional RNA library Prep kit for Illumina
352 (New England Biolabs), and read in paired-end 40-cycle sequencing runs on the NextSeq 500
353 system (Illumina). Sequences were aligned to the Ensembl *Mus musculus* GRCm38.83.chr.gtf
354 genome (mm10) assembly using HISAT2 v2.0.5 (PMID: 25751142), sorted and indexed using
355 SAMtools v1.7 (39) and quantified for differential expression analysis using Subread v1.6.1
356 featureCounts (40). Differential expression analysis was performed using DESeq2 v1.18.1 (41,
357 42). Enriched canonical pathways were identified using the Ingenuity pathways analysis software

358 (QIAGEN). Gene Ontology (GO) analysis excluding inferred electronic annotations, was
359 performed using the Mouse Genome Informatics GO Browser and GO Term Mapper
360 (http://www.informatics.jax.org). Genes encoding mouse nuclear hormone receptors were
361 obtained from the Nuclear Receptor Signaling Atlas (NURSA) (43). Genes encoding
362 mitochondrial proteins were obtained from the mouse Mitocarta2.0 (22, 44). Genes encoding
363 transcriptional coregulators were obtained from the EpiFactors database (45). Glucocorticoid-
364 responsive genes were obtained by combining previously published datasets (46) reanalyzed with
365 GEO2R, with other dexamethasone-regulated genes that we identified in C2C12 myotubes, GEO
366 accession no. GSE149453. Heatmaps were prepared using Pheatmap v1.0.8, RColorBrewer v1.1–
367 2, and other software packages available in R. Other data visualizations were performed using
368 GraphPad Prism7.
369

370 **Glucose uptake**

371 Insulin mediated 2-deoxy-D-[^{14}C] glucose uptake was determined by incubating primary
372 myotubes with PBS or PBS containing 100 nM insulin for 30 min followed by addition of 0.1 mM
373 of cold 2-deoxy-D-glucose and 0.1µCi/well of 2-deoxy-[^{14}C] D-glucose for 5 min prior to
374 solubilization. Nonspecific deoxyglucose uptake was measured in the presence of 20 µM
375 cytochalasin B and subtracted from the total glucose uptake.
376

377 **Primary myoblast isolation and culture**

378 Primary myoblasts were isolated from P1 to P3 (1–3 day old) C57BL/6J pups as described
379 (Springer *et al*, 1997) and cultured on collagen coated plates in media consisting in 1:1 F-
380 10/DMEM supplemented with 20% FCS and 25 µg/ml bFGF. Subconfluent myoblasts were

381 differentiated into multinucleated myotubes using a 1:1 F-10/5 mM glucose DMEM supplemented
382 with 4% heat inactivated horse serum (Hyclone) for up to five days. For steroid-free culture
383 conditions, cells were grown in charcoal:dextran-stripped FBS (Gemini Bio-products, cat no. 100-
384 119).
385
386 **Adenoviruses**
387 Control GFP-expressing and Crtc2 expressing adenoviruses have been described (Koo *et al*, 2005;
388 Wu *et al*, 2006). For all experiments myotubes were infected after 72 hr of differentiation with
389 4×10^8 viral particles per ml per well for 24–48 hr.
390
391 **Immunoblotting analysis**
392 Immunoblot analysis was performed as described (Conkright *et al*, 2003a). Whole cell extracts
393 were prepared in HEPES whole cell lysis buffer (20 mM HEPES, pH 7.4, 1% TX-100,1x
394 phosphoSTOP complete inhibition cocktail tablets [Roche], and 1X Complete-EDTA Free
395 protease inhibitor cocktail [Roche]). Frozen muscle tissue was homogenized in lysis buffer T-
396 PER® Tissue Protein Extraction reagent (Thermo Scientific) by a polytron homogenizer and
397 sonication. The protein concentration was determined using the protein assay reagent (Bio-Rad).
398 60–80 μg of protein were separated by SDS-PAGE and transferred to nitrocellulose membranes
399 for immunoblotting. Nur77/Nr4a1 #2518 Rabbit polyclonal antibody was from Novus Biological.
400 CRTC2 #A300-638A Rabbit polyclonal antibody was from Bethyl Laboratories. Irs2 (L1326)
401 #3089S Rabbit polyclonal antibody was Cell Signaling Technology, Inc. Tubulin #T9026-.2ML
402 Mouse Monoclonal antibody was from Sigma-Aldrich. pAKT(Thr308) (244f1)Rb and

403 pAKT(Ser473) (971s) were from Cell Signaling Technology. PGC1α ab54481 Rb was from
404 Abcam.
405
406 **Quantitative RT-PCR (qPCR)**
407 Total RNA from tissue or cells was harvested using Rneasy RNA Kit (Qiagen) and cDNA prepared
408 using Transcriptor High Fidelity cDNA Synthesis Kit (Roche). Relative abundance of cDNAs was
409 determined a Roche LightCycler 480, and the resulting data were normalized to *Rpl-23* ribosomal
410 RNA (IDT) as described (Conkright *et al*, 2003b). The primer pairs are as follows: *Nr4a1* (5′-
411 ttctgctcaggcctggtact′, 5′-gattctgcagctcttccacc-3′); *Nr4a3* (5′-tcagccttttggagctgtt′, 5′-
412 tgaagtcgatgcaggacaag-3′); *Irs2* (5′-acaacctatcgtggcacctc-3′, 5′-gacggtggtggtagaggaaa-3′); Idh3a
413 (5′-gtgacaagaggttttgctggt-3′, 5′-tgaaatttctgggccaattc-3′); *Cytc* (5′-gatgccaacaagaacaaaggt-3′, 5′-
414 tgggattttccaaatactccat-3′); *Glut4* (5′-tgtggctgtgccatcttg-3′, 5′-cagggccaatctcaaagaag-3′).
415
416 **Mitochondrial DNA (mt-DNA) analysis**
417 Total DNA was extracted using the GenElute™ mammalian genomic DNA miniprep kit (Sigma-
418 Aldrich). Triplicate real-time PCR reactions were performed using 50 ng of total DNA, *CoxI* (5′-
419 agcattcccacgaataaataaca-3′, 5′-agcattcccacgaataaataacat-3′) or *CoxII* (5′-tttcaacttggcttacaagacg-3′,
420 5′-tttcaacttggcttacaagacg-3′) mitochondrial DNA primers, and a control genomic DNA primer,
421 *Gapdh* (5’-gaaaaggagattgctacg-3’, 5’-gcaagaggctaggggc-3’).
422

423 **Histology**

424 Dissected muscle tissue was mounted in OCT medium (TissueTek) and froze in liquid N_2–cooled
425 isopentane. Tissue sections were stained for succinate dehydrogenase activity to distinguish
426 between oxidative and nonoxidative fibers using standard methods.

427

428 **Fatty acid metabolism**

429 Fatty acid oxidation was assayed by incubating (9,10(n)-^{3}H) palmitic acid (60 Ci/mmol) bound to
430 fatty-acid free albumin (final concentration:100 μM, palmitate:albumin 2:1) and 1 mM carnitine
431 with primary myocytes for 2 hr. Tritiated water released was collected and quantitated.

432

433 **High-content imaging and analysis**

434 Primary or C2C12 myotubes in black 96- or 384-well tissue culture plates with clear bases (Greiner
435 Bio-One, North America, Inc.) were stained for 15 min with 200 nM MitoTracker® Orange CM-
436 H_2TMRos dye (Invitrogen™ by ThermoFisher Scientific). The myotubes were rinsed with steroid-
437 free DMEM to remove un-incorporated dye, and then incubated in the differentiation media for 45
438 min to reach peak fluorescence. Myotubes were fixed in 4% formaldehyde for 20 min, stained with
439 300 nM DAPI for 5 min, permeabilized in PBS containing 0.1% Triton X-100 for 20 min, blocked
440 for 1 h with 1x TBS containing 0.1% Tween-20 (TBS-T) and 2.5% normal goat serum, and
441 incubated at 4°C overnight with an AlexaFluor® 488-conjugated anti-skeletal muscle myosin (F59)
442 antibody (Santa Cruz Biotechnology, Inc. cat no. sc-32732 AF488). The next day, the myotubes
443 were washed 4 times with TBS-T to remove unbound antibodies and rinsed twice with PBS. The
444 stained myotubes were imaged at 10–20X magnification on the IN Cell Analyzer 6000 platform
445 (GE Healthcare). For each treatment condition, a stack of 24–27 images containing an average of

50–100 myotubes per image were analyzed using the IN Cell Developer Toolbox image analysis software, with a customized segmentation protocol for myotubes. The average (mean) diameter and mitochondrial potential (i.e. MitoTracker staining density x area) of myotubes in these images were then calculated.

Data Availability

The raw and processed RNA-seq dataset is freely available to the public at the National Center for Biotechnology Information (NCBI) Gene Expression Omnibus (GEO) https://www.ncbi.nlm.nih.gov/geo/ and can be retrieved with the accession number GSE149150, which will be released upon publication of this manuscript. The processed RNA-seq dataset is also provided in SI Appendix, **Dataset S1**. Relevant protocols and raw data not detailed in the Methods or Supplementary Information are available upon request.

Acknowledgements. N.E.B. was supported by the BallenIsles Men's Golf Association. J.C.N. was supported by the Frenchman's Creek Women for Cancer Research.

Author contributions Conceptualization, N.E.B., M.D.C., K.W.N.; Methodology, N.E.B., M.D.C.; Investigation, N.E.B., J.C.N., S.S., R.H., D.S.; Writing – Original Draft, K.W.N., N.E.B., M.D.C., S.H., S.S.S.; Writing – Revision, K.W.N, J.C.N., N.E.B.; Supervision, M.D.C, G.L.H., K.W.N., S.S.S., N.E.B.

References

1. C. L. Melby, H. L. Paris, R. M. Foright, J. Peth, Attenuating the Biologic Drive for Weight Regain Following Weight Loss: Must What Goes Down Always Go Back Up? *Nutrients* **9** (2017).
2. M. Rosenbaum *et al.*, Effects of experimental weight perturbation on skeletal muscle work efficiency in human subjects. *Am J Physiol Regul Integr Comp Physiol* **285**, R183-192 (2003).
3. L. J. Arone, R. Mackintosh, M. Rosenbaum, R. L. Leibel, J. Hirsch, Autonomic nervous system activity in weight gain and weight loss. *Am J Physiol* **269**, R222-225 (1995).
4. M. Rosenbaum *et al.*, Low-dose leptin reverses skeletal muscle, autonomic, and neuroendocrine adaptations to maintenance of reduced weight. *J Clin Invest* **115**, 3579-3586 (2005).
5. R. M. Foright *et al.*, Is regular exercise an effective strategy for weight loss maintenance? *Physiol Behav* **188**, 86-93 (2018).
6. P. S. MacLean *et al.*, Regular exercise attenuates the metabolic drive to regain weight after long-term weight loss. *Am J Physiol Regul Integr Comp Physiol* **297**, R793-802 (2009).
7. Y. Turk *et al.*, High intensity training in obesity: a Meta-analysis. *Obesity science & practice* **3**, 258-271 (2017).
8. A. Mourier *et al.*, Mobilization of visceral adipose tissue related to the improvement in insulin sensitivity in response to physical training in NIDDM. Effects of branched-chain amino acid supplements. *Diabetes care* **20**, 385-391 (1997).
9. M. Rosenbaum *et al.*, Resistance Training Reduces Skeletal Muscle Work Efficiency in Weight-Reduced and Non-Weight-Reduced Subjects. *Obesity (Silver Spring)* **26**, 1576-1583 (2018).
10. D. M. Ostendorf *et al.*, Physical Activity Energy Expenditure and Total Daily Energy Expenditure in Successful Weight Loss Maintainers. *Obesity (Silver Spring)* **27**, 496-504 (2019).
11. D. A. Walsh, J. P. Perkins, E. G. Krebs, An adenosine 3',5'-monophosphate-dependant protein kinase from rabbit skeletal muscle. *The Journal of biological chemistry* **243**, 3763-3765 (1968).
12. R. A. Screaton *et al.*, The CREB coactivator TORC2 functions as a calcium- and cAMP-sensitive coincidence detector. *Cell* **119**, 61-74 (2004).
13. N. E. Bruno *et al.*, Creb coactivators direct anabolic responses and enhance performance of skeletal muscle. *The EMBO journal* **33**, 1027-1043 (2014).
14. T. H. Ch'ng *et al.*, Activity-dependent transport of the transcriptional coactivator CRTC1 from synapse to nucleus. *Cell* **150**, 207-221 (2012).
15. P. S. Baxter, M. A. Martel, A. McMahon, P. C. Kind, G. E. Hardingham, Pituitary adenylate cyclase-activating peptide induces long-lasting neuroprotection through the induction of activity-dependent signaling via the cyclic AMP response element-binding protein-regulated transcription co-activator 1. *J Neurochem* **118**, 365-378 (2011).
16. M. Taub, S. Garimella, D. Kim, T. Rajkhowa, F. Cutuli, Renal proximal tubule Na,K-ATPase is controlled by CREB-regulated transcriptional coactivators as well as salt-inducible kinase 1. *Cell Signal* **27**, 2568-2578 (2015).

510 17. Z. Wu *et al.*, Transducer of regulated CREB-binding proteins (TORCs) induce PGC-1alpha
511 transcription and mitochondrial biogenesis in muscle cells. *Proc Natl Acad Sci U S A* **103**,
512 14379-14384 (2006).
513 18. N. D. Knuth *et al.*, Metabolic adaptation following massive weight loss is related to the
514 degree of energy imbalance and changes in circulating leptin. *Obesity (Silver Spring)* **22**,
515 2563-2569 (2014).
516 19. J. C. Kerns *et al.*, Increased Physical Activity Associated with Less Weight Regain Six
517 Years After "The Biggest Loser" Competition. *Obesity (Silver Spring)* **25**, 1838-1843
518 (2017).
519 20. R. J. Verheggen *et al.*, A systematic review and meta-analysis on the effects of exercise
520 training versus hypocaloric diet: distinct effects on body weight and visceral adipose tissue.
521 *Obes Rev* **17**, 664-690 (2016).
522 21. R. Goldsmith *et al.*, Effects of experimental weight perturbation on skeletal muscle work
523 efficiency, fuel utilization, and biochemistry in human subjects. *Am J Physiol Regul Integr*
524 *Comp Physiol* **298**, R79-88 (2010).
525 22. S. E. Calvo, K. R. Clauser, V. K. Mootha, MitoCarta2.0: an updated inventory of
526 mammalian mitochondrial proteins. *Nucleic Acids Res* **44**, D1251-1257 (2016).
527 23. V. Giorgio *et al.*, Dimers of mitochondrial ATP synthase form the permeability transition
528 pore. *Proc Natl Acad Sci U S A* **110**, 5887-5892 (2013).
529 24. A. S. Rambold, B. Kostelecky, N. Elia, J. Lippincott-Schwartz, Tubular network formation
530 protects mitochondria from autophagosomal degradation during nutrient starvation. *Proc*
531 *Natl Acad Sci U S A* **108**, 10190-10195 (2011).
532 25. V. Nasta, D. Suraci, S. Gourdoupis, S. Ciofi-Baffoni, L. Banci, A pathway for assembling
533 [4Fe-4S](2+) clusters in mitochondrial iron-sulfur protein biogenesis. *FEBS J*
534 10.1111/febs.15140 (2019).
535 26. J. Liu *et al.*, Mitochondrial Dysfunction Launches Dexamethasone-Induced Skeletal
536 Muscle Atrophy via AMPK/FOXO3 Signaling. *Mol Pharm* **13**, 73-84 (2016).
537 27. D. Ratman *et al.*, Chromatin recruitment of activated AMPK drives fasting response genes
538 co-controlled by GR and PPARalpha. *Nucleic Acids Res* **44**, 10539-10553 (2016).
539 28. G. R. Steinberg *et al.*, Reduced glycogen availability is associated with increased
540 AMPKalpha2 activity, nuclear AMPKalpha2 protein abundance, and GLUT4 mRNA
541 expression in contracting human skeletal muscle. *Appl Physiol Nutr Metab* **31**, 302-312
542 (2006).
543 29. B. Dasgupta *et al.*, The AMPK beta2 subunit is required for energy homeostasis during
544 metabolic stress. *Mol Cell Biol* **32**, 2837-2848 (2012).
545 30. B. R. Barnes *et al.*, The 5'-AMP-activated protein kinase gamma3 isoform has a key role
546 in carbohydrate and lipid metabolism in glycolytic skeletal muscle. *The Journal of*
547 *biological chemistry* **279**, 38441-38447 (2004).
548 31. C. S. Choi *et al.*, Paradoxical effects of increased expression of PGC-1alpha on muscle
549 mitochondrial function and insulin-stimulated muscle glucose metabolism. *Proc Natl Acad*
550 *Sci U S A* **105**, 19926-19931 (2008).
551 32. M. Tadaishi *et al.*, Skeletal muscle-specific expression of PGC-1alpha-b, an exercise-
552 responsive isoform, increases exercise capacity and peak oxygen uptake. *PLoS One* **6**,
553 e28290 (2011).
554 33. R. P. Shook *et al.*, Moderate cardiorespiratory fitness is positively associated with resting
555 metabolic rate in young adults. *Mayo Clin Proc* **89**, 763-771 (2014).

556 34. M. Gilliat-Wimberly, M. M. Manore, K. Woolf, P. D. Swan, S. S. Carroll, Effects of
557 habitual physical activity on the resting metabolic rates and body compositions of women
558 aged 35 to 50 years. *J Am Diet Assoc* **101**, 1181-1188 (2001).
559 35. J. C. Drake, R. J. Wilson, Z. Yan, Molecular mechanisms for mitochondrial adaptation to
560 exercise training in skeletal muscle. *FASEB J* **30**, 13-22 (2016).
561 36. M. A. Pearen, G. E. Muscat, Minireview: Nuclear hormone receptor 4A signaling:
562 implications for metabolic disease. *Mol Endocrinol* **24**, 1891-1903 (2010).
563 37. M. A. Maxwell *et al.*, Nur77 regulates lipolysis in skeletal muscle cells. Evidence for cross-
564 talk between the beta-adrenergic and an orphan nuclear hormone receptor pathway. *The*
565 *Journal of biological chemistry* **280**, 12573-12584 (2005).
566 38. J. Meinken, G. Walker, C. R. Cooper, X. J. Min, MetazSecKB: the human and animal
567 secretome and subcellular proteome knowledgebase. *Database (Oxford)* **2015** (2015).
568 39. H. Li *et al.*, The Sequence Alignment/Map format and SAMtools. *Bioinformatics* **25**, 2078-
569 2079 (2009).
570 40. Y. Liao, G. K. Smyth, W. Shi, featureCounts: an efficient general purpose program for
571 assigning sequence reads to genomic features. *Bioinformatics* **30**, 923-930 (2014).
572 41. M. I. Love, W. Huber, S. Anders, Moderated estimation of fold change and dispersion for
573 RNA-seq data with DESeq2. *Genome Biol* **15**, 550 (2014).
574 42. S. Anders, W. Huber, Differential expression analysis for sequence count data. *Genome*
575 *Biol* **11**, R106 (2010).
576 43. R. N. Margolis, R. M. Evans, B. W. O'Malley, N. A. Consortium, The Nuclear Receptor
577 Signaling Atlas: development of a functional atlas of nuclear receptors. *Mol Endocrinol*
578 **19**, 2433-2436 (2005).
579 44. D. J. Pagliarini *et al.*, A mitochondrial protein compendium elucidates complex I disease
580 biology. *Cell* **134**, 112-123 (2008).
581 45. Y. A. Medvedeva *et al.*, EpiFactors: a comprehensive database of human epigenetic factors
582 and complexes. *Database (Oxford)* **2015**, bav067 (2015).
583 46. T. Kuo *et al.*, Genome-wide analysis of glucocorticoid receptor-binding sites in myotubes
584 identifies gene networks modulating insulin signaling. *Proc Natl Acad Sci U S A* **109**,
585 11160-11165 (2012).
586

587

588 **FIGURES**

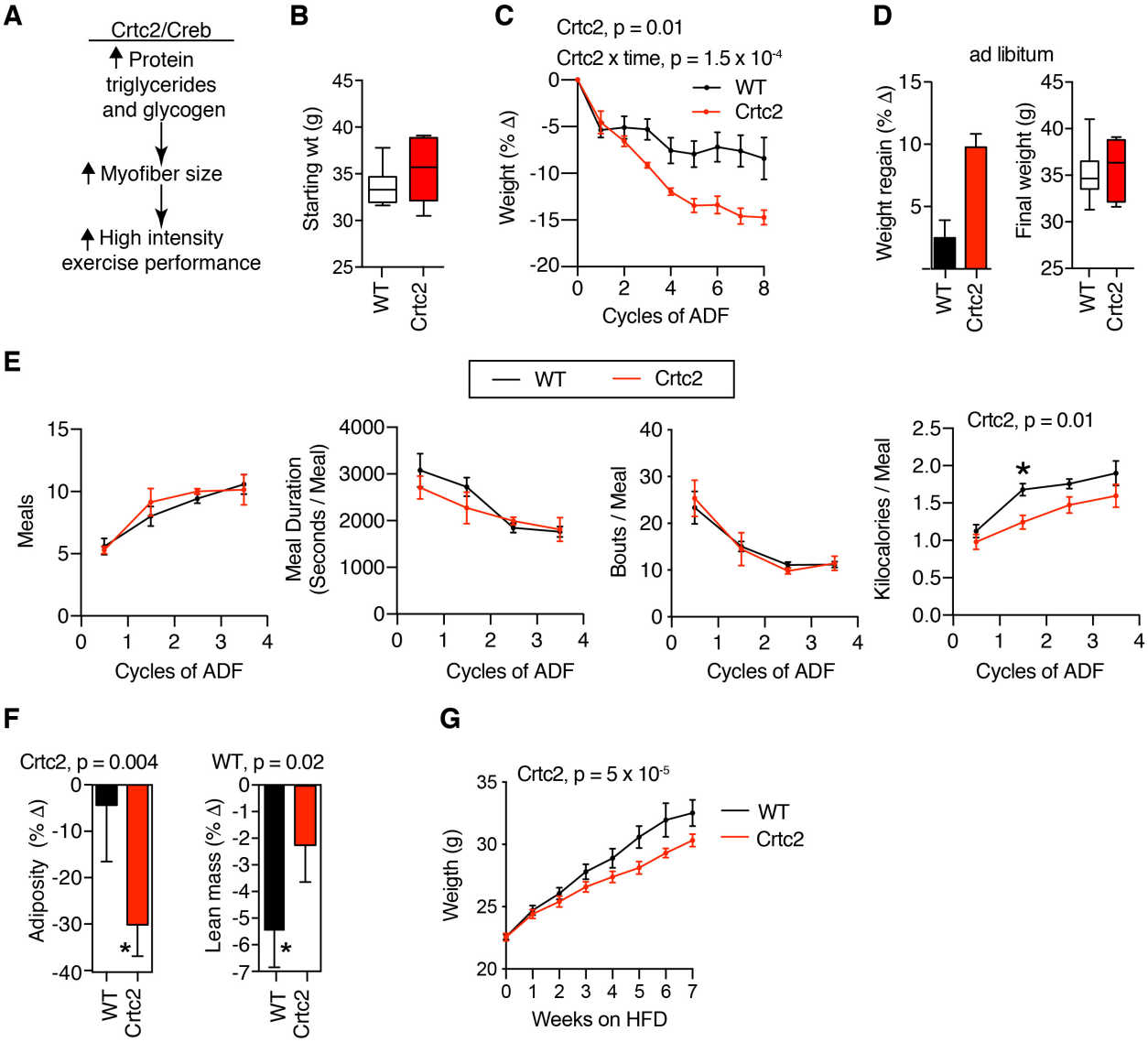

589

590 **Figure 1. Crtc2/Creb1 signaling enables greater loss of weight and adiposity during alternate**
591 **day fasting (ADF).**

592 (**A**) Summary of previous work showing that Crtc2 overexpression produced an exercised
593 phenotype (13).

594 (**B**) 18-week old C57BL/6 male control (WT) and Crtc2 mice were treated with dox for 35 days
595 and weighed. Data are shown as box-and-whisker plot, indicating the middle quartiles and
596 range. $N = 6$ (WT) or 5 (Crtc2) mice per group.

597 (**C-F**) Mice from (**B**) were subject to alternate day fasting (ADF).

598 (**C**) Changes in the body weight during ADF.

599 (**D**) Weight regain after the ADF treatment and 3 weeks of ad libitum feeding. *significant in
600 Sidak's test for planned comparisons.
601 (**E**) Behaviors were assayed with Biodak monitoring system, including number of meals, bouts per
602 meal, meal duration, and kilocalories consumed over the 12-hr re-feeding period.
603 (**F**) Adiposity and lean mass determined by whole-body NMR measurements taken before and
604 after 8 cycles of ADF.
605 (**G**) 8-week old C57BL/6 male control and Crtc2 mice were treated with dox and placed on a high
606 fat diet (HFD). $N = 9$ (WT) or 7 (Crtc2) mice per group
607 Data are shown as mean ± SEM.
608

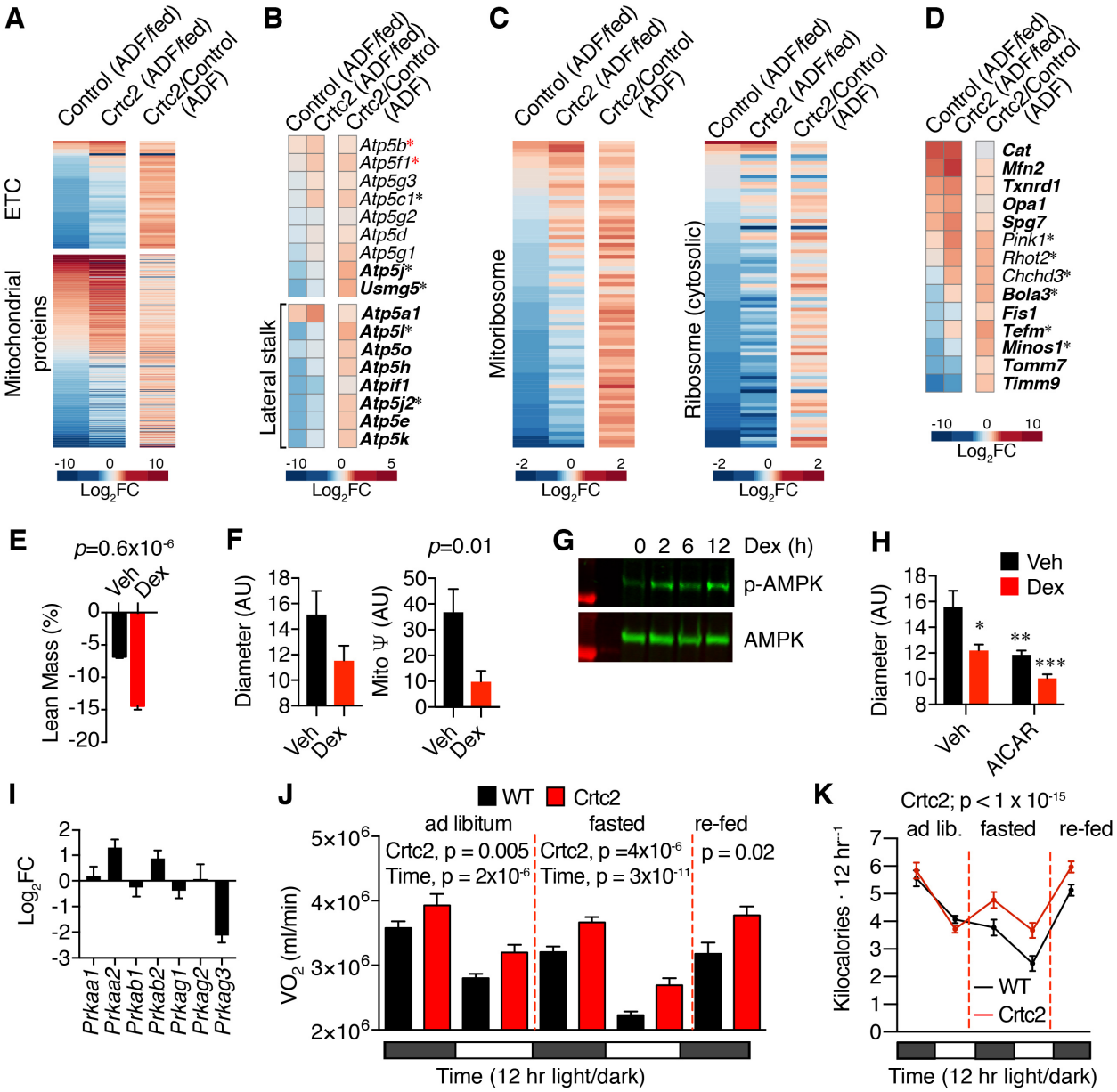

Figure 2. Electron transport chain gene expression and whole-body energy expenditure regulation by weight loss and fasting is reversed by Crtc2 expression.

(**A**–**D**) Gene expression profiles in control and Crtc2-transduced TA muscles of mice subjected to ADF relative to the ad libitum fed mice (columns 1–2), and effect of Crtc2 transduction relative to control during ADF (column 3). The profiles of all genes encoding **A**) mitochondrial proteins, including subunits of electron transport chain (ETC) complexes, **B**) subunits of the mitochondrial ATPase (complex V), **C**) ribosomal subunits, and **D**) highlighted mitochondrial proteins, are shown. ADF-regulated genes in control muscle appear

618 in **bold**. *Crtc2-regulated genes in mice subjected to ADF. *ADF-regulated genes in Crtc2-
619 transduced muscle but not control. FC, fold change.
620 (**E**) Effects of Dex on lean body mass. Mice injected with vehicle or 10 mg/kg Dex were fasted
621 overnight. Lean mass was measured by whole-body NMR before and after treatment. *N* = 5
622 mice per group.
623 (**F**) Diameter and mitochondrial potential of steroid-deprived primary myotubes treated for 2 days
624 with vehicle or 100 nM Dex were compared by confocal high-content imaging. *N* = 24–27
625 images x 50–100 myotubes per image.
626 (**G**) Steroid-deprived C2C12 myotubes were stimulated with 100 nM Dex for 0–12 h. Levels of
627 phosphorylated and total AMPK in whole lysates were compared by western blot.
628 (**H**) Diameter of steroid deprived C2C12 myotubes treated for 48 h with vehicle, 100 nM Dex, or
629 1 uM AICAR were compared by confocal high content imaging. *N* = 24–27 images x 50–100
630 myotubes per image.
631 (**I**) Expression levels of genes encoding AMPK subunits in mice described in **Figure 2**.
632 (**J**) VO_2 and VCO_2 were measured continuously (**Figure S2A**) for 72 hrs. in a CLAMS animal
633 monitoring system. Shown are the 12-hr averages. *N* = 8 mice per group.
634 (**K**) Total energy expenditure was calculated from VO_2 and VCO_2 values using the Lusk equation.
635 Data are shown as mean ± SEM.

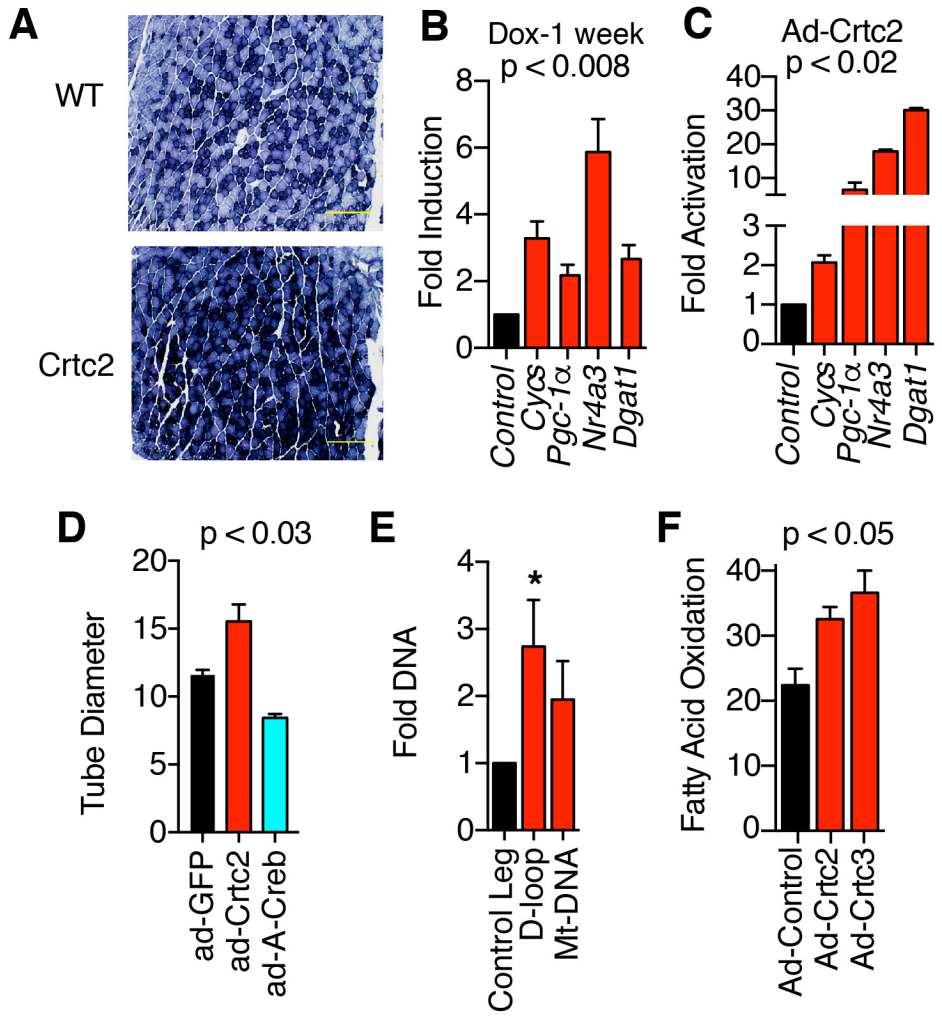

Figure 3. Crtc2 expression in skeletal muscle enhances mitochondrial biogenesis.

(**A**) Expression profiles of genes that regulate lipid metabolism in mice described in **Figure 2.**

(**B**) Histological analysis of succinate dehydrogenase in myofibers from gastrocnemius muscle sections after dox treatment. Scale bar = 500 μm.

(**C**) Gene induction calculated relative to WT mice. *N* = 8 mice per group.

(**D**) Gene expression in primary myocytes transduced with adenovirus expressing Crtc2 or GFP control 72 hr post-transduction.

(**E**) C2C12 myocytes were transduced with adenovirus GFP, Crtc2, or A-Creb genes and analyzed by confocal high content imaging. *N* = 24–27 images x 50–100 myotubes per image.

(**F**) Crtc2 expression plasmid was electroporated into the tibialis anterior muscle and GFP plasmid in the contralateral leg. After 7 days, DNA was extracted for assessment of mitochondrial DNA (mt-DNA) for Crtc2/GFP control. *N* = 5 mice per group.

649 (**G**) Oxidation of ^{3}H-Palmitic acid in the supernatant of primary myocytes transduced with control,
650 Crtc2, or Crtc3-expressing adenovirus.
651 * $p < 0.05$. Data are shown as mean + SEM.
652

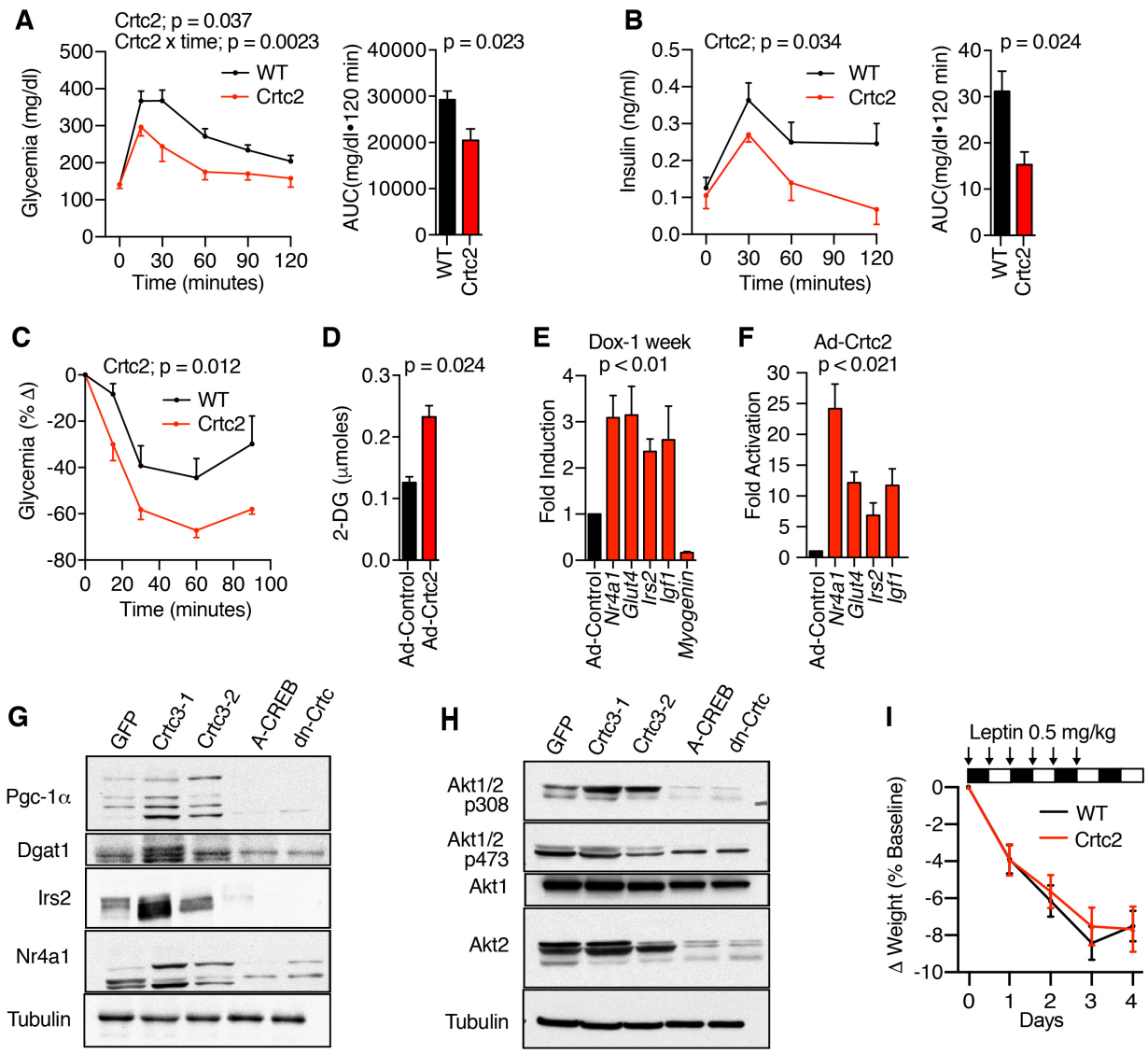

Figure 4. Crtc2 transgenic mice maintain enhanced glucose disposal and insulin tolerance

(**A**) Expression profiles of genes that regulate carbohydrate metabolism in mice described in **Figure 2**.

(**B**) Glucose tolerance test (GTT) after alternate day fasting. Right panel, area under the curve. *N* = 10 mice per group

(**C**) Plasma insulin levels during GTT described in panel **B**.

(**D**) Insulin tolerance tests after 8 cycles of ADF. *N* = 10 mice per group

(**E**) Insulin-mediated uptake of 2-deoxy-D-glucose in primary myocytes transduced with adenovirus expressing Crtc2 or GFP control. *N* = 10 per group. Student's t-test.

(**F**) Crtc2 mice were treated +/- dox for 1 week and the gene induction compared by qPCR relative

664 to the no dox groups. N= 10 per group.

665 (**G**) Gene expression in primary myocytes transduced with adenovirus expressing Crtc2 or GFP
666 control were compared by qPCR. *N*=4 per group.

667 (**H**) Western blot of whole lysates from primary myocytes transduced with the indicated plasmids.

668 (**I–J**) Myocytes stably expressing GFP, Crtc3 (lanes 2 and 3), dominant negative Creb (A-CREB),
669 or dominant negative Crtc2 (dn-Crtc) were compared by western blots.

670 (**K**) WT or Crtc2 mice were injected twice daily with 0.5 mg/kg leptin and weight was monitored.
671 *N*=8 mice per group.

672 Data are mean ± SEM.

673

674

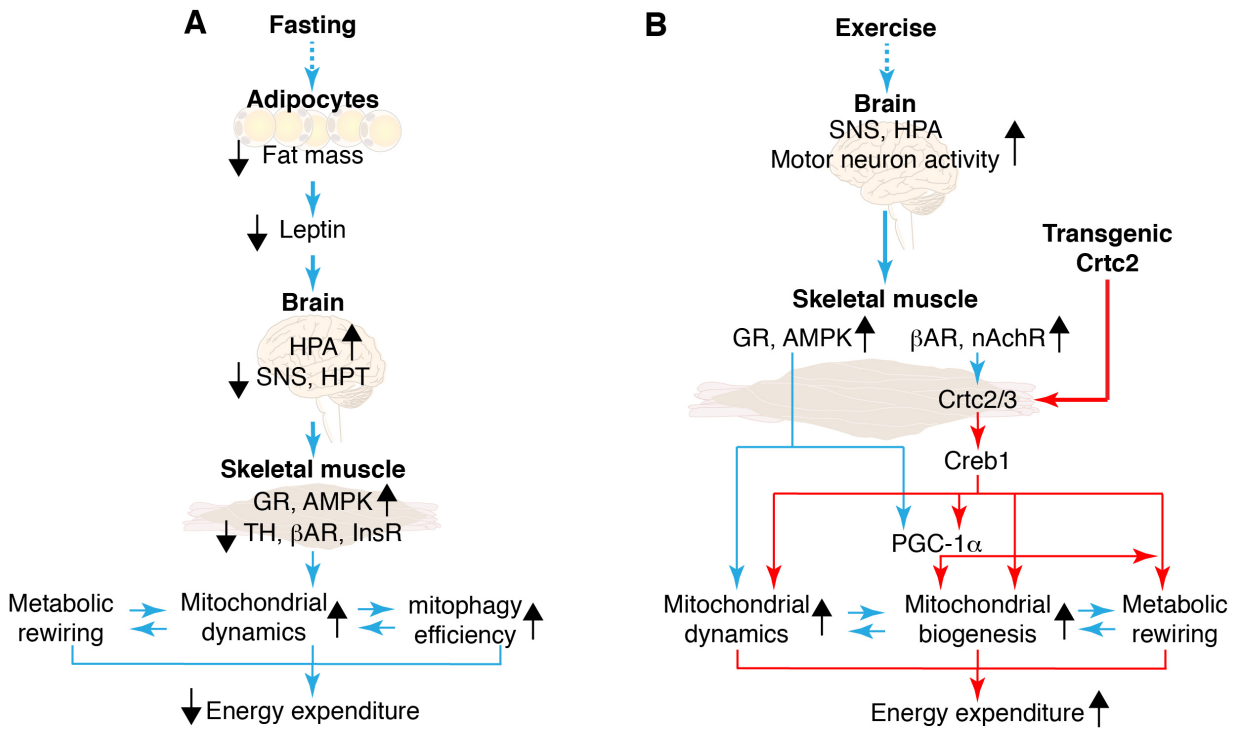

Figure 5. Hormonal and neural modulation of energy expenditure in skeletal muscle

(**A**) Fasting-induced regulation of mitochondrial dynamics and mitophagy.

(**B**) Exercise-induced regulation of mitochondrial dynamics and mitochondrial biogenesis, which can be constitutively activated by overexpression of Crtc2 in skeletal muscle.

bAR, b-adrenergic receptor; GR, glucocorticoid receptor; HPA, hypothalamic-pituitary-adrenal axis; HPT, hypothalamic-pituitary-thyroid axis; InsR, insulin receptor; nAchR, nicotinic acetylcholine receptor; SNS, sympathetic nervous system; TH, thyroid hormone